LAWRENCE
LIVERMORE
NATIONAL
LABORATORY

LLNL-JRNL-407523

Regional Multi-station Discriminants: Magnitude, Distance and Amplitude Corrections and Sources of Error

D. N. Anderson, W. R. Walter, D. K. Fagan, T. M. Mercier, S. R. Taylor

October 7, 2008

Bulletin of the Seismological Society of America

Disclaimer

Regional Multi-station Discriminants: Magnitude, Distance and Amplitude Corrections and Sources of Error

(PNNL-SA-49313)

Submitted to the *Bulletin of the Seismological Society of America*

D.N. Anderson
Pacific Northwest National Laboratory†
W.R. Walter
Lawrence Livermore National Laboratory
D.K. Fagan T.M. Mercier
Pacific Northwest National Laboratory
S.R. Taylor
Rocky Mountain Geophysics, LLC

Summary. Magnitude, distance and amplitude corrections (MDAC) made to observed regional amplitudes are necessary so that what remains in the corrected amplitude is mostly information about the seismic source-type. Corrected amplitudes can be used in ratios to discriminate between earthquakes and explosions. However, there remain source effects such as those due to depth, focal mechanism, local material property and apparent stress variability that cannot easily be determined and applied as amplitude corrections. We develop a mathematical model to capture these near source effects as random (unknown) giving an error partition of three sources: model inadequacy, station noise and amplitude correlations. This mathematical model is the basis for a general multi-station regional discriminant formulation. The standard error of the discriminant includes these three sources of error in its formulation. The developed methods are demonstrated with a collection of Nevada Test Site (NTS) events observed at regional stations. Importantly, the proposed formulation includes all corrected amplitude information through the construction of multi-station discriminants. In contrast, previous studies have only computed discriminants from single stations having both P and S amplitudes. The proposed multi-station approach has similarities to the well established m_b versus M_s discriminant and represents a new paradigm for the regional discrimination problem.

1. Introduction

The ratio of regional P and S wave amplitude measurements at high frequencies can discriminate between earthquakes and explosions (e.g. Walter et al. (1995); Taylor (1996); Bottone et al. (2002)). An issue with using these amplitudes in a practical application is how to remove the effects due to path, site and magnitude to emphasize the source differences. In Taylor and Hartse (1998), Taylor et al. (2002) and Walter and Taylor (2002) the Magnitude and Distance Amplitude Correction (MDAC) technique corrects each regional phase (e.g. P_n, P_g, S_n, L_g) amplitude as a function of frequency in an attempt to make amplitudes independent of distance, magnitude and station. MDAC is a simple physically based model that accounts for propagation effects such as geometrical spreading and Q, and corrects observed amplitudes assuming the scaling of an earthquake spectral model developed by Brune (1970). The idea of using an earthquake MDAC model to correct amplitudes is that spectra from an explosion will exhibit a poor fit to the model which will be apparent in an observed discriminant. Because of complex explosion source phenomenology it is not necessarily obvious which combinations of regional phases will best separate earthquake and explosion populations. The MDAC technique allows the formulation of any combination of regional phases in any frequency band, so that a diversity of discriminants can be explored.

In our development, the MDAC model for an event is assumed to be a known physical correction equation – a function of frequency and distance only. The MDAC model partitions regional seismic spectra into component parts. The instrument-corrected regional phase spectra can be thought of as a convolution between the source-type and the path. In the frequency domain this can be mathematically represented as

$$A(\omega, \Delta) = S(\omega)G(\Delta)P(\omega)B(\omega, \Delta) \tag{1}$$

where S is the source spectrum, G is geometrical spreading, P is the frequency-dependent site effect, and B is the anelastic attenuation with function arguments epicentral distance Δ and angular frequency ω. Here we have split the path effect into three components: 1) a frequency independent geometrical spreading component, 2) a range independent and frequency dependent site effect, and 3) an anelastic attenuation component.

The logarithm of both sides of Equation (1) gives

$$\log A(\omega, \Delta) = \log S(\omega) + \log G(\Delta) + \log P(\omega) + \log B(\omega, \Delta). \quad (2)$$

To remove distance and magnitude trends in the data, we correct the observed spectrum $\log A_o(\omega, \Delta)$ so that

$$Y = \log A_c(\omega, \Delta) = \log A_o(\omega, \Delta) - \log A(\omega, \Delta), \quad (3)$$

where $Y = \log A_c(\omega, \Delta)$ is the corrected spectrum (MDAC residual). Equation (3) is used to calculate corrected MDAC amplitudes Y that are then used to construct discriminants.

We develop the mathematics to form a multi-station discriminant constructed from the station average of the corrected amplitudes Y. The proposed discriminant is built from random effects analysis of variance (Searle (1971) and Searle et al. (1992)) which has been applied to other path correction theories in seismology (e.g., Chen and Tsai (2002), Tsai and Chen (2003) and Tsai et al. (2006)). We model any remaining physical structure in corrected amplitudes as a source-type bias plus two random effect components – model inadequacy and station noise. This approach to discriminant formulation properly forms the standard error of the discriminant with these two variance components. Model inadequacy decreases with improvements in amplitude correction theory and improved calibration (e.g., improved MDAC parameters). Station noise is reduced through station averaging. MDAC (or any other path correction formulation) can be augmented with additional corrections and the multi-station model developed here holds.

A compelling argument for using all available station information with the multi-station discriminant is illustrated with a thought experiment: Four stations observe signals from a clandestine nuclear explosion. Three of the four stations only observe the P wave (which may be the case for an explosion). The fourth station observes both P and S. The P wave at the fourth station is anomalously low causing the discriminant to appear earthquake-like resulting in a miss-classified explosion if only this station is used (for example it is *a priori* determined to have the best identification performance of the four). However, if all of the corrected P wave amplitudes are averaged and combined with the single S wave measurement, a better estimate of the actual P/S ratio is obtained and the event is correctly identified. The multi-station discriminant developed here is a technically rigorous approach to resolve this apparent conflict among individual station identifications because it properly combines the corrected station amplitudes with mathematical statistics theory.

We compared individual station performance reported in Walter et al. (1995) to the multi-station discriminant performance using a comparable MDAC model and data. Walter et al. (1995) report equi-probable error rates of 13.4% and 18.1% for Kanab, Utah and Mina, Nevada respectively. The multi-station discriminant exhibits improved performance with an equi-probable error rate slightly less than 10%. We also validate the multi-station discriminant with an analysis of model assumptions in Section 3. Section 4 demonstrates that the multi-station discriminant is also applicable to other amplitude correction methods used in discrimination analysis, specifically regression corrections on station discriminants. In Section 5, we present the results of a cross-validation study that compares the multi-station discriminant performance to that of a best single station identification method. The cross-validation analysis demonstrates significant improved performance with the multi-station discriminant. We note that the same MDAC correction is used throughout this paper.

The multi-station regional discriminant is analogous to the formulation of the m_b versus M_s discriminant used for decades in seismic event identification (see Blandford (1982)). To see this, we note that the calculation of a corrected amplitude (Equation (3)) is very similar to the calculation of a station m_b or M_s. In the m_b versus M_s discriminant, station-averaged magnitudes are used with potentially differing sets of stations in the calculation of each. Similarly, the multi-station regional discriminant proposed here is constructed from station-averaged corrected amplitudes also with potentially differing stations used in each.

2. The MDAC Discriminant: Model Inadequacy and Station Noise

Until now, no attempt has been made to obtain a realistic estimate of the error budget associated with corrected amplitudes. Established signal processing research treats amplitudes as lognormal distributed and therefore, in log space, properly formed differences are normal (Gaussian) discriminants. The conceptual representation of the proposed model is

$$Y = \log(\text{corrected amplitude}) = Bias(\text{source-type}) + Event + Noise \tag{4}$$

where $Bias$(source-type) is a source-type constant, $Event$ is a zero mean random effect that varies from event to event and represents model inadequacy from effects such as depth, focal mechanism, local material property and apparent stress variability, and $Noise$ represents measurement and ambient noise, also with zero mean. The MDAC approach results in a $Bias$ term for earthquakes

that is near zero, whereas for explosions the $Bias$ is non-zero indicating discrimination potential. Equation (4) implies the expected value of Y is

$$\mathcal{E}\{Y\} = Bias(\text{source-type}). \tag{5}$$

For the mathematical statistics formulation of Equation (4), define the random variable Y_{ijk} to be the corrected amplitude for source-type $i = 0, 1$ (earthquake, explosion), event j and station k (observed data are denoted y_{ijk}). The linear model representation of Equation (4) is then

$$Y_{ijk} = \mu_i + E_j + \epsilon_{(ij)k} \quad j = 1, 2, \ldots m_i \quad k = 1, 2, \ldots n_{ij}. \tag{6}$$

Analogous to Equation (4), Equation (6) reads Y_{ijk} equals a constant source-type bias μ_i plus a random event adjustment E_j (model inadequacy due to local source effects) plus a station noise adjustment $\epsilon_{(ij)k}$. The E_j are modeled as independent Gaussian random variables with zero mean and variance τ^2. The $\epsilon_{(ij)k}$ are independent Gaussian random variables with zero mean and variance σ^2. E_j and $\epsilon_{(ij)k}$ are independent across all subscripts. This assumption is consistent with effects local to the source being uncorrelated with station noise. The subscript notation $(ij)k$ for ϵ simply specifies that *observed* station noise is different for each source-type, event and station. However, the probability model for $\epsilon_{(ij)k}$ is identical for each source-type, event and station. Equation (6) is a standard mixed effects (random and fixed) linear model (see Searle (1971) and Searle et al. (1992)).

As an example, for two stations and three events the statistical properties of E_j and $\epsilon_{(ij)k}$ are succinctly written as

$$\begin{pmatrix} E_1 \\ \epsilon_{(i1)1} \\ \epsilon_{(i1)2} \\ E_2 \\ \epsilon_{(i2)1} \\ \epsilon_{(i2)2} \\ E_3 \\ \epsilon_{(i3)1} \\ \epsilon_{(i3)2} \end{pmatrix} \text{ is Gaussian } (\underline{0}, \Sigma), \quad \Sigma = \begin{pmatrix} \tau^2 & 0 & 0 & 0 & 0 & 0 & 0 & 0 & 0 \\ 0 & \sigma^2 & 0 & 0 & 0 & 0 & 0 & 0 & 0 \\ 0 & 0 & \sigma^2 & 0 & 0 & 0 & 0 & 0 & 0 \\ 0 & 0 & 0 & \tau^2 & 0 & 0 & 0 & 0 & 0 \\ 0 & 0 & 0 & 0 & \sigma^2 & 0 & 0 & 0 & 0 \\ 0 & 0 & 0 & 0 & 0 & \sigma^2 & 0 & 0 & 0 \\ 0 & 0 & 0 & 0 & 0 & 0 & \tau^2 & 0 & 0 \\ 0 & 0 & 0 & 0 & 0 & 0 & 0 & \sigma^2 & 0 \\ 0 & 0 & 0 & 0 & 0 & 0 & 0 & 0 & \sigma^2 \end{pmatrix}, \tag{7}$$

where $\underline{0}$ denotes a zero mean vector and Σ is the covariance matrix of the model error components.

Define the indicator matrix

$$W = \begin{pmatrix} 1 & 1 & 0 & 0 & 0 & 0 & 0 & 0 & 0 \\ 1 & 0 & 1 & 0 & 0 & 0 & 0 & 0 & 0 \\ 0 & 0 & 0 & 1 & 1 & 0 & 0 & 0 & 0 \\ 0 & 0 & 0 & 1 & 0 & 1 & 0 & 0 & 0 \\ 0 & 0 & 0 & 0 & 0 & 0 & 1 & 1 & 0 \\ 0 & 0 & 0 & 0 & 0 & 0 & 1 & 0 & 1 \end{pmatrix} \tag{8}$$

to select appropriate vector/matrix elements for the matrix representation of Equation (6). Then

$$\begin{pmatrix} Y_{i11} \\ Y_{i12} \\ Y_{i21} \\ Y_{i22} \\ Y_{i31} \\ Y_{i32} \end{pmatrix} = \begin{pmatrix} \mu_i \\ \mu_i \\ \mu_i \\ \mu_i \\ \mu_i \\ \mu_i \end{pmatrix} + \begin{pmatrix} 1 & 1 & 0 & 0 & 0 & 0 & 0 & 0 & 0 \\ 1 & 0 & 1 & 0 & 0 & 0 & 0 & 0 & 0 \\ 0 & 0 & 0 & 1 & 1 & 0 & 0 & 0 & 0 \\ 0 & 0 & 0 & 1 & 0 & 1 & 0 & 0 & 0 \\ 0 & 0 & 0 & 0 & 0 & 0 & 1 & 1 & 0 \\ 0 & 0 & 0 & 0 & 0 & 0 & 1 & 0 & 1 \end{pmatrix} \begin{pmatrix} E_1 \\ \epsilon_{(i1)1} \\ \epsilon_{(i1)2} \\ E_2 \\ \epsilon_{(i2)1} \\ \epsilon_{(i2)2} \\ E_3 \\ \epsilon_{(i3)1} \\ \epsilon_{(i3)2} \end{pmatrix} \text{ is Gaussian } (\underline{\theta}, \Omega) , \tag{9}$$

where the mean vector $\underline{\theta}$ and covariance matrix Ω are

$$\underline{\theta} = \begin{pmatrix} \mu_i \\ \mu_i \\ \mu_i \\ \mu_i \\ \mu_i \\ \mu_i \end{pmatrix} \text{ and } \Omega = W\Sigma W' = \begin{pmatrix} \tau^2 + \sigma^2 & \tau^2 & 0 & 0 & 0 & 0 \\ \tau^2 & \tau^2 + \sigma^2 & 0 & 0 & 0 & 0 \\ 0 & 0 & \tau^2 + \sigma^2 & \tau^2 & 0 & 0 \\ 0 & 0 & \tau^2 & \tau^2 + \sigma^2 & 0 & 0 \\ 0 & 0 & 0 & 0 & \tau^2 + \sigma^2 & \tau^2 \\ 0 & 0 & 0 & 0 & \tau^2 & \tau^2 + \sigma^2 \end{pmatrix} . \tag{10}$$

This two station and three event example is easily generalized across source-types i, events $j = 1, 2, \ldots, m_i$ and stations $k = 1, 2, \ldots, n_{ij}$.

2.1. Statistical Properties of a Station-Averaged MDAC Residual

For source-type i and event j, denote the $1 \times n_{ij}$ vector of corrected amplitudes as $\underline{Y}'_{ij} = (Y_{ij1}, Y_{ij2}, \ldots, Y_{ijn_{ij}})$. Then generalizing to n_{ij} stations, $\underline{Y}_{ij}$ is multivariate normal with $1 \times n_{ij}$ mean vector $\underline{\theta}'_{ij} = (\mu_i, \mu_i, \ldots, \mu_i)$ and $n_{ij} \times n_{ij}$ covariance matrix

$$\Omega_{ij} = \begin{pmatrix} \tau^2+\sigma^2 & \tau^2 & \tau^2 & \cdots & \tau^2 \\ \tau^2 & \tau^2+\sigma^2 & \tau^2 & & \tau^2 \\ \tau^2 & \tau^2 & \ddots & & \vdots \\ \vdots & & & \tau^2+\sigma^2 & \tau^2 \\ \tau^2 & \cdots & \tau^2 & \tau^2 & \tau^2+\sigma^2 \end{pmatrix}. \tag{11}$$

The station-averaged corrected amplitude $\bar{Y}_{ij} = \underline{\mathbf{1}}'\underline{Y}_{ij}/n_{ij}$ is normal with mean μ_i and standard error $\tau^2 + \sigma^2/n_{ij}$. $\underline{\mathbf{1}}$ is a $1 \times n_{ij}$ vector of 1s. Note that forming regional discriminants from station-averaged corrected amplitudes exactly parallels the methodology of the m_b versus M_s discriminant where both are station-averaged magnitudes.

Omitting the term E_j in Equation (6) implies that the corrected amplitude at a station is μ_i plus station noise. As demonstrated with the following argument, this model formulation is fundamentally inconsistent with the realities of seismic observation. The standard error of $\bar{Y}_{ij}$ with E_j removed from Equation (6) is σ^2/n_{ij} ($\tau^2 = 0$) and decreases as the number of stations n_{ij} observing an event increases. This implies that if enough stations observe an event, this standard error effectively goes to zero and the average corrected amplitude quickly converges to μ_i implying near-perfect discrimination capability. By not including the term E_j, effects such as depth, focal mechanism, local material property and apparent stress variability are not accounted for in the theoretical model of an amplitude, and clearly these effects cannot be removed by station averaging. The model given by Equation (6) captures these local source effects by admitting that they cannot be mathematically (theoretically) represented. Treating local source effects as a random effect (E_j) compensates for them as a component in the standard error of a discriminant. Also, the lower bound of Equation (6) is non-zero and therefore consistent with realistic seismic monitoring.

Another important property of this model is the correlation between station amplitudes for an event. The correlation ($\tau^2/(\tau^2+\sigma^2)$) implies that large adjustment E_j increases correlation between stations because this random adjustment is applied to all stations observing an event, that is, the

stations stochastically move together with near source model error. Small adjustment E_j implies the correction model is good and is conceptually equivalent to stations with incoherent noise. Small adjustment E_j also implies τ^2 is small and the standard error of $\bar{Y}_{ij}$ is reduced further through station averaging.

In contrast to the correlation between station amplitudes, correlation between station averaged amplitudes used to form a discriminant is easily introduced into Equation (6). Two station averaged amplitudes $\bar{Y}_{ij}$ and $\bar{Y}^*_{ij}$ are used to construct regional discriminants and they can be correlated. For example, $\bar{Y}_{ij}$ could be an average P wave amplitude and $\bar{Y}^*_{ij}$ an average S wave amplitude. The MDAC correction removes magnitude from amplitudes and so the correlation between station averaged amplitudes used to form a discriminant is due to the correlation between model *error* terms E_j. An observed model error E_j for P_g is linearly related to observed E_j for L_g with the correlation indicating the scatter around the line of the relationship. Conceptually extending the example given in Equation (7) to two amplitudes gives a block diagonal covariance matrix with the $(1,1)$ block for Y_{ijk} and the $(2,2)$ block for Y^*_{ijk}. Introducing a correlation ρ (covariance) in the off-diagonal blocks between the E terms for Y_{ijk} and Y^*_{ijk} provides the statistical model to calculate the standard error of the multi-station discriminant given in Section 2.2. Calibration data y_{ijk} and y^*_{ijk} are from events observed by stations for both source-types. For the analysis examples in Sections 3 and 4, and the cross validation study Section 5, established methods are used to estimate the variance components (τ, σ) and amplitude correlation (ρ) (see for example Searle (1971) and Searle et al. (1992)).

2.2. Discriminant Formulation

A discriminant is constructed from two different station-averaged amplitudes $\bar{Y}_{ij}$ and $\bar{Y}^*_{ij}$ (with different bias constants μ_i and μ^*_i). For specific regional phases the discriminant equation can be represented with meaningful subscripts. For example, for a given event with source-type i, the station-averaged corrected amplitude $\bar{P}_g$ is normal with mean μ_{i,P_g} and standard error $\tau^2_{P_g} + \sigma^2_{P_g}/n_{P_g}$ and $\bar{L}_g$ is normal with mean μ_{i,L_g} and standard error $\tau^2_{L_g} + \sigma^2_{L_g}/n_{L_g}$. Note that if only stations observing a discriminant are used, then $n_{P_g} = n_{L_g}$, however, this constraint on discriminant construction is not necessary – using all available data to construct a discriminant is theoretically sound with good instrument and amplitude corrections. With the inclusion of correlation ρ between

amplitudes used to form a discriminant, the standard error of the P_g versus L_g discriminant is

$$SE_{\bar{P}_g - \bar{L}_g} = \sqrt{\tau^2_{P_g} + \frac{\sigma^2_{P_g}}{n_{P_g}} + \tau^2_{L_g} + \frac{\sigma^2_{L_g}}{n_{L_g}} - 2\,\rho\,\tau_{P_g}\,\tau_{L_g}} \tag{12}$$

for both earthquakes and explosions. Equality of the standard error for both source types is an important model property because unlike discrimination analysis with unequal source-type variability, it ensures that an earthquake with an unusually strong earthquake-identifying discriminant will not be identified as an explosion. For example, quadratic discrimination (unequal source-type variance) gives an explosion density function for such a discriminant that is larger than the earthquake density function, and therefore incorrectly identifies the event as an explosion.

Current physical correction theory is unable to adjust amplitudes for all local effects. Section 3 demonstrates removal of magnitude from amplitudes with MDAC, however a clear correlation between observed MDAC amplitudes is shown which agrees well with the introduction of the amplitude correlation ρ into the multi-station model Equation (6). Local physical corrections not captured in MDAC are modeled as random and as discussed previously these local effects move out to all stations (and therefore amplitudes), hence the correlations. When physical corrections for local effects are possible, the model inadequacy terms E_j will be small, giving small values of τ, and the covariance between station amplitudes will be small. In the limit, this conceptually gives discriminant amplitude scatter plots for explosions and earthquakes (populations) that are small shotgun patterns of data and the discrimination problem becomes one of physical correction and station noise.

Centering the multi-station discriminant relative to some constant and adjusting for uncertainty gives a standardized discriminant. For example, centering relative to the explosion population mean $\mu_{1,P_g} - \mu_{1,L_g}$ forms the standardized discriminant

$$Z_{\bar{P}_g - \bar{L}_g} = \frac{(\bar{P}_g - \mu_{1,P_g}) - (\bar{L}_g - \mu_{1,L_g})}{\sqrt{\tau^2_{P_g} + \sigma^2_{P_g}/n_{P_g} + \tau^2_{L_g} + \sigma^2_{L_g}/n_{L_g} - 2\,\rho\,\tau_{P_g}\,\tau_{L_g}}}. \tag{13}$$

which is centered at zero for explosions and has a non-zero center for earthquakes. Equation (6) mathematically formalizes the MDAC approach to regional discrimination and bases source-type identification performance fundamentally on differences between the bias constants μ_i and μ_i^*. The advantage to centering relative to explosions is consistency with the monitoring position to assume all events are explosions and then prove otherwise with seismic signatures.

Equation (6) also implies that $Z_{\bar{P}_g-\bar{L}_g}$ has the same variance for both populations. As noted above, imposing equal population variances is driven by physical basis considerations so that an explosion with an unusually strong explosion-identifying discriminant value will not be identified as an earthquake as could be the case with quadratic discrimination rules.

From Equation (13), values of $Z_{\bar{P}_g-\bar{L}_g}$ less than a decision threshold predict earthquake as the source-type identification, otherwise explosion. Section 3 illustrates performance with two decision thresholds; a model-based threshold that gives equal missed-explosion and false-alarm error rates and an empirical decision threshold. The model-based threshold is the average of the means of $Z_{\bar{P}_g-\bar{L}_g}$ for explosions and earthquakes. The empirical-based threshold is simply the average of largest earthquake Z and the smallest explosion Z. The empirical-based decision threshold is derived from the tail behavior of the observed data and can be strongly influenced by the empirical distribution of the calibration data. The model-based threshold is derived from the fit of model parameters to calibration data. In Sections 3 and 4 we provide both to illustrate the difference.

3. NTS Data Analysis with the MDAC Multi-Station Discriminant

The data used to illustrate the discriminant $Z_{\bar{P}_g-\bar{L}_g}$ (Equation (13)) are events at and surrounding the Nevada Test Site (NTS). Data quality metrics ensure high quality observed amplitudes. These metrics include signal to noise, station coverage and elimination of events incongruent with regional phases. Discrimination with regional phases presumes that earthquakes with depths incongruent to regional phases have been removed from identification consideration. This data quality requirement is very important to the analysis that follows supporting equal variability for earthquake and explosion discriminant populations. Events were observed with combinations of four seismic stations: Kanab, Utah (KNB); Elko, Nevada (ELK), Landers, California (LAC) and Columbia College, California (CMB). MDAC amplitudes from these stations were averaged in the calculation of $Z_{\bar{P}_g-\bar{L}_g}$. P_g and L_g amplitudes were pseudo spectral measurements with a 6 to 8 Hertz filter window. After applying data quality metrics (e.g., signal to noise and removal of events within 100 kilometers of a station), the data table consisted of 41 earthquakes (EQ) and 159 explosions (EX) for a total of 200 events. Moment magnitudes (M_w) ranged from 2.6 to 6.1 for earthquakes, and 2.8 to 5.9 for explosions. The spatial distribution of the events and stations is presented in Figure 1.

Amplitude corrections for discrimination remove the effects of magnitude and distance so that

what remains in the corrected amplitude is fundamentally information about source type. Figure 2 demonstrates the removal of the effect of moment magnitude M_w from the P_g and L_g amplitudes with MDAC. Note that the earthquakes are mean centered to zero. With amplitude corrections, there is often correlation between the amplitudes used to form a discriminant. Figure 3(a) shows MDAC corrected P_g and L_g data for earthquakes and explosions. The earthquake data exhibit more L_g energy consistent with the physical basis of the P_g versus L_g discriminant. The model Equation (6) assumes that the earthquake and explosion populations have equal covariance matrices for all events and the calibration data under this assumption are given in Figure 3(b). These data are used to compute the model parameters for Equation (6).

For both earthquakes and explosions E_j and $\epsilon_{(ij)k}$ are modeled as zero mean with variances τ^2 and σ^2 respectively. The assumption that the model terms E_j and $\epsilon_{(ij)k}$ are uncorrelated is conceptually valid because E_j represents source model inadequacy and stations (and therefore station noise) are at least 100 kilometers from the source. Fitting Equation (6) to the NTS data in Figure 3(b) provides calculated values of E_j and $\epsilon_{(ij)k}$. The distributional properties of these calculated model terms is provided in Figure 4. The χ^2 goodness-of-fit tests confirm that E_j and $\epsilon_{(ij)k}$ are reasonably modeled as normal random variables. The $\epsilon_{(ij)k}$ for L_g (Figure 4(f)) have individual χ^2 values for the tail cells that are unusually large and with these removed the goodness-of-fit test returned $\chi^2 = 8.05$ with 3 degrees of freedom and p-value ≈ 0.04. This test indicates that the $\epsilon_{(ij)k}$ for L_g exhibits some kurtosis, however the residuals are reasonably bell shaped and are consistent with the normal assumption. Figure 5 gives quantile-quantile (Q-Q) plots that further confirm that E_j and $\epsilon_{(ij)k}$ are reasonably modeled as normal random variables. The 95% confidence bounds on the Q-Q plots are simulated (Lilliefors (1967)). Figure 6 empirically shows the correlation between model inadequacy E_j for the two discriminant amplitudes. These data provide a value of 0.95 for the model parameter ρ.

The fitted population models for $Z_{\bar{P}_g - \bar{L}_g}$ with equal (pooled) variance of 0.48 are presented in Figure 7. A goodness-of-fit test applied to the explosion population returned $\chi^2 = 16.28$ with 15 degrees of freedom and p-value = 0.36. A goodness-of-fit test applied to the earthquake population returned $\chi^2 = 13.31$ with 15 degrees of freedom and p-value = 0.58. These two tests indicate that the equal population variance and normal assumptions for Equation (6) is reasonable.

Estimated model parameters are provided in Tables 1 and 2. Using the fitted models, the decision threshold is $\ell_{Model} = -0.89$. From the receiver operation characteristic (ROC) curve in

Figure 8, the equi-probable error is $\approx 10\%$. The empirical decision threshold is $\ell_{Empirical} = -1.27$. Figure 9 is a plot of the observed discriminants $Z_{\bar{P}_g - \bar{L}_g}$ versus M_w, with $\ell_{Empirical}$ and ℓ_{Model}. The empirical-based decision threshold is derived from the tail behavior of the observed data and can be strongly influenced by the empirical distribution of the calibration data. The model-based threshold is derived from the fit of model parameters to calibration data. The performance from Figure 9 is provided in Tables 3 and 4. In this analysis, performance is reported as apparent (see McLachlan (1992)), that is, all data were used to calculate model parameters and then discrimination analysis, using all data, was performed with these same parameters. In Section 5 the MDAC multi-station discriminant is shown to have better performance than that of a best single station approach with a comprehensive cross-validation study.

Figure 9 suggests the possibility of a correlation between Z and M_w for explosions. There is well-documented dependence of the P_g versus L_g discriminant on material properties at NTS (see Figure 6 in Walter et al. (1995)). Explosions detonated below the water table in high-strength media have larger P_g versus L_g values than those detonated above the water table in lower strength media (see Figure 10 in Walter et al. (1995)). Containment practices at NTS dictate that larger explosions are conducted at greater depths. Therefore, M_w is actually acting as a surrogate for a rapid change in material properties occurring near the water table encountered by larger and more deeply buried explosions. The apparent differences in compression to shear energy scaling for explosions and earthquakes is also observed in published (and widely used) developments of the m_b versus M_s discriminant (see Stevens and Day (1985), Taylor (1996) and Bonner et al. (2006)). The apparent correlation between Z and M_w is fundamentally due to sampling bias for the explosion population – there are no large shallow explosions and no small deep explosions in this data set. Were the explosion population to have these events, the apparent correlation would not be present. Even with this sampling bias, the assumptions for Equation (6) are valid as demonstrated in the previous paragraphs – both the earthquake and explosion populations can be reasonably modeled as bivariate normal with normal marginal distributions.

4. NTS Data Analysis with a Regression Correction Multi-Station Discriminant

Prior to the MDAC formulation, discriminants were formed by first calculating a spectral ratio in a common frequency band at each station observing the event (see Blandford (1982)). These station-

centric discriminants are known to be robust to instrument response calibration and this calculation also removes the effect of magnitude. In the literature, station discriminants are then corrected for distance with a regression model built from earthquake calibration data (see Hartse et al. (1997) and Bottone et al. (2002)). Analogous to the development in Section 2, define the random variable X_{ijk} to be the regression corrected station discriminant for source-type $i = 0, 1$ (earthquake, explosion), event j and station k (observed station discriminants are denoted x_{ijk}). Then

$$X_{ijk} = \mu_i + E_j + \epsilon_{(ij)k} \quad j = 1, 2, \ldots m_i \quad k = 1, 2, \ldots n_{ij}. \tag{14}$$

For an event with n_X station discriminants, the event discriminant is the average of station discriminants $\bar{X}_{ij}$ and the standard error is

$$SE_{\bar{X}} = \sqrt{\tau^2 + \frac{\sigma^2}{n_X}} \tag{15}$$

for both earthquakes and explosions. Note that in the multi-station discriminant, n_{P_g} and n_{L_g} amplitudes are averaged. Centering relative to the explosion population mean $\mu_{1,X}$ forms the standardized discriminant

$$Z_{\bar{X}} = \frac{\bar{X} - \mu_{1,X}}{\sqrt{\tau^2 + \frac{\sigma^2}{n_X}}}. \tag{16}$$

which is centered at zero for explosions and has a non-zero center for earthquakes.

In the context of this paper we calculate the difference of the observed station amplitudes P_g and L_g. We then distance correct these station discriminants with Δ and $\log \Delta$ as regressor variables (see Hartse et al. (1997) and Bottone et al. (2002)). Applying this regression model to all events gives distance corrected station discriminants X_{ijk} – the residuals. The fitted population models for $Z_{\bar{X}}$ are presented in Figure 10. Estimated model parameters are provided in Tables 5 and 6. Using these fitted models, the decision threshold is $\ell_{Model} = -1.16$. From the receiver operation characteristic (ROC) curve in Figure 8, the equi-probable error is $\approx 12.5\%$. The empirical decision threshold is $\ell_{Empirical} = -1.80$. Figure 11 is a plot of the observed discriminants $Z_{\bar{P}_g - \bar{L}_g}$ versus M_w, with $\ell_{Empirical}$ and ℓ_{Model}. The performance from Figure 11 is provided in Tables 7 and 8. Like the MDAC analysis in Section 3, performance is apparent. Note that the sampling characteristics of the explosion population discussed in Section 3 are also prevalent with regression corrected station

discriminants. The MDAC approach has slightly better performance than the regression correction approach presented in this section – 7/159 missed explosions versus 9/159 with an empirical decision line and 2/41 false alarms versus 11/41 with an empirical decision line. Missed explosions are a serious error in the context of the treaty verification standard to "miss no explosions", and from this perspective the MDAC multi-station discriminant is a promising regional discriminant formulation.

There are two important differences between the MDAC and distance regression approach to correction, and associated multi-station discriminant formulation. First, the MDAC multi-station discriminant uses all available amplitudes from an event to calculate the station averaged amplitudes forming the discriminant. In contrast, only those stations observing a discriminant are used in the multi-station regression approach. Second, the MDAC correction is optimally tuned, specific to phase and frequency, to station and path with earthquake calibration data. In contrast, the regression correction, also constructed with earthquake calibration data, has no station and path specificity in the mathematics.

5. Cross-Validation Analysis: MDAC Multi-station Discriminant versus Best Single-Station

We performed a cross-validation study to demonstrate that the multi-station discriminant results in improved performance over a best single-station approach. A third approach was also investigated and compared: for events not observed by the best single-station, it used information from the other stations to make an event identification. We have called this approach "single-station plus."

The figure of merit used in our analysis is operational burden per correctly identified explosion which is conceptually a false discovery rate (FDR). Operational burden has two components; the probability of identifying an earthquake as an explosion, and the probability of being unable to determine source type because of missing measurements. In either case, an event would require further analysis. Specifically,

$$\mathrm{FDR} = \frac{P(\hat{EX} \mid EQ) + P(\hat{NoID} \mid EX) + P(\hat{NoID} \mid EQ)}{P(\hat{EX} \mid EX)}, \tag{17}$$

where $P(\hat{A} \mid B)$ is the probability an event is identified as source type A given the true source type is B, and $\hat{NoID}$ indicates that an identification was not possible.

To ensure direct comparison, all amplitudes used in the cross-validation study were MDAC corrected. The study consisted of 5000 iterations. For each, a random sample of 80% of the events

was selected from the NTS data. These data represent historic or calibration events and provided the measurments to calculate the necessary multi-station discriminant parameters (τ and σ for P_g and L_g, and ρ) for both populations, and decision rules (lines) for the three discrimination approaches. For each approach the variability was assumed equal for both source types, giving a linear discrimination decision rule for all three. In the calibration component of an iteration, data are used to compute discriminant parameters, then with these parameters in hand event discriminants are calculated and decision rules are developed. For the multi-station discriminant, $Z_{\bar{P}_g - \bar{L}_g}$ values are calculated. For both of the single-station approaches, only the station discriminant $X = P_g - L_g$ is calculated (e.g., no station averaging). The decision rule (line) for the multi-station discriminant is simply the mean of the two source type means, that is, $(\bar{Z}_{EX} + \bar{Z}_{EQ})/2$. For the single-station approaches, the decision rule (line) for each station is calculated as $(\bar{X}_{EX} + \bar{X}_{EQ})/2$, and with this decision rule an FDR can be calculated for each station. The best single-station is then the one with the lowest FDR. Ties were broken by choosing the station with the highest $P(\hat{EX} \mid EX)$.

The remaining 20% of events in each iteration served as test data and can be viewed as new events requiring identification analysis. The discriminant parameters calculated from the 80% calibration data were used to compute the discriminants for the test data events and then the decision rules developed from the calibration events were applied. If a test event is not observed by the best single-station an identification is not possible. In the single-station plus approach, if an event is not observed by the best single-station, the decisions from the remaining stations are used – a simple vote with the majority providing the event identification. If only one of the remaining stations sees the new event, its decision is used as the event identification. If the remaining stations are in conflict (no majority), then no-identification ($NoID$) is logged. For all three approaches, the predicted source type was then compared to the true type.

FDR results are summarized in Figure 12. One can see the multi-station discriminant far outperforms the single-station approach and also represents an improvement over the single-station plus approach. The results of a closer look with FDR for only the multi-station and single-station plus approaches are presented in Figure 13. The two FDR components are operational burden in the numerator and probability of correctly identifying an explosion in the denominator. FDR is reduced as operational burden decreases. The part of operational burden resulting from no-identification is summarized in Figure 14. The results emphasize a serious limitation of the single-station approaches – an unacceptably high no-identification rate. Because data from all stations are used in the multi-

station discriminant, source type can be predicted for all events. The other part of operational burden comes from the probability of calling an earthquake an explosion. These results are summarized in Figure 15, and suggest that the performance of the single-station approach is slightly better than the other two approaches.

FDR is reduced as the $P(\hat{EX} \mid EX)$ increases. These results are summarized in Figure 16. Here, the multi-station discriminant has significantly better performance than the single-station approach, and also represents an improvement over the single-station plus approach.

6. Summary

We have developed and demonstrated a new approach to the regional seismic discrimination problem for nuclear explosion monitoring. In many ways, the method is analogous to that of the m_b versus M_s discriminant that has been in use for many decades. The idea is to individually correct observed station phase amplitudes, as a function of frequency, for path and earthquake source scaling using MDAC. Resulting amplitude corrections are then averaged over all observing stations prior to forming a ratio. This approach contrasts sharply with that of computing a phase ratio discriminant at individual stations. In the latter case, only stations that observe both phases or amplitudes are used thereby excluding many potential measurements at additional stations. Research to develop regional amplitude-based discriminants for nuclear explosion monitoring has focused on theory development for seismic amplitude corrections. This paper develops a general model for corrected amplitudes that properly includes correction model inadequacy and station noise as sources of error. This random effects model correctly gives the standard error of a multi-station discriminant with a lower bound that conforms to physical basis, that is, the standard error will not become unrealistically small with an increase in observing stations. No source and path correction method is perfect and model inadequacy is always present in a discriminant. Future work includes the use of maximum likelihood (ML) magnitudes (Ringdal (1976)) for the regional multi-station and m_b versus M_s discriminant, and development of error budgets for each which will result in standard errors analogous to Equation (12).

Acknowledgments

The authors acknowledge the support of Ms. Leslie A. Casey and the National Nuclear Security Administration Office of Nonproliferation Research and Development for funding this work. This work was completed under the auspices of the U.S. Department of Energy by Pacific Northwest National Laboratory under contract DE-AC05-76RL01830. The authors acknowledge the technical advise and historical perspective of Robert Blandford and Robert Shumway. The authors express appreciation to anonymous reviewers for excellent critique and comment.

Prepared by LLNL under Contract DE-AC52-07NA27344.

References

Blandford, R. (1982). Seismic event discrimination. *Bulletin of the Seismological Society of America*, 72:69–87.

Bonner, J., Russell, D., Harkrider, D., Reiter, D., and Herrmann, R. (2006). Development of a time-domain, variable-period surface-wave magnitude measurement procedure for application at regional and teleseismic distances, Part II: Application and $M_s - m_b$ performance. *Bulletin of the Seismological Society of America*, 96:678–696.

Bottone, S., Fisk, M., and McCartor, G. (2002). Regional seismic-event characterization using a bayesian formulation of simple kriging. *Bulletin of the Seismological Society of America*, 92:2277–2296.

Brune, J. (1970). Tectonic stress and the spectra from seismic shear waves earthquakes. *J. Geophys. Res.*, 75:4997–5009.

Chen, Y. and Tsai, P. (2002). A new method of estimation of the attenuation relationship with variance components. *Bulletin of the Seismological Society of America*, 92:1984–1991.

Hartse, H., Taylor, S., Phillips, W., and Randall, G. (1997). Regional event discrimination in central Asia with emphasis on western China. *Bulletin of the Seismological Society of America*, 87:551–568.

Lilliefors, H. (1967). On the Kolmogorov-Smirnov test for normality with mean and variance unknown. *Journal of the American Statistical Association*, 62:399–402.

McLachlan, G. (1992). *Discriminant Analysis and Statistical Pattern Recognition*. John Wiley & Sons, New York.

Ringdal, F. (1976). Maximum likelihood estimation of seismic magnitude. *Bulletin of the Seismological Society of America*, 66:789–802.

Searle, S. (1971). *Linear Models*. John Wiley & Sons, New York.

Searle, S., Casella, G., and McCulloch, C. (1992). *Variance Components*. John Wiley & Sons, New York.

Stevens, J. and Day, S. (1985). The physical basis of the mb:Ms and variable frequency magnitude methods for earthquake/explosion discrimination. *J. Geophys. Res.*, 90:3009–3020.

Taylor, S. (1996). Analysis of high-frequency Pg/Lg ratios from nts explosions and western u.s. earthquakes. *Bulletin of the Seismological Society of America*, 86:1042–1053.

Taylor, S. and Hartse, H. (1998). A procedure for estimation of source and propagation amplitude corrections for regional seismic discriminants. *J. Geophys. Res.*, 103:2781–2789.

Taylor, S., Velasco, A., Hartse, H., Phillips, W., Walter, W., and Rodgers, A. (2002). Amplitude corrections for regional seismic discriminants. *Pure. App. Geophys.*, 159:623–650.

Tsai, P. and Chen, Y. (2003). Reduction of ground motion variability using the variance components technique. *EOS Trans. AGU*, 84.

Tsai, P., Chen, Y., and Chia-Hsin, L. (2006). The path effect in ground-motion variability: An application of the variance-components technique. *Bulletin of the Seismological Society of America*, 96:1170–1176.

Walter, W., Mayeda, K., and Patton, H. (1995). Phase and spectral ratio discrimination between nts earthquakes and explosions part 1: Empirical observations. *Bulletin of the Seismological Society of America*, 85:1050–1067.

Walter, W. and Taylor, S. (2002). A revised magnitude and distance amplitude correction (MDAC2) procedure for regional seismic discriminants: Theory and testing at NTS. Technical Report LAUR-02-1008, Los Alamos National Laboratory, Los Alamos, New Mexico.

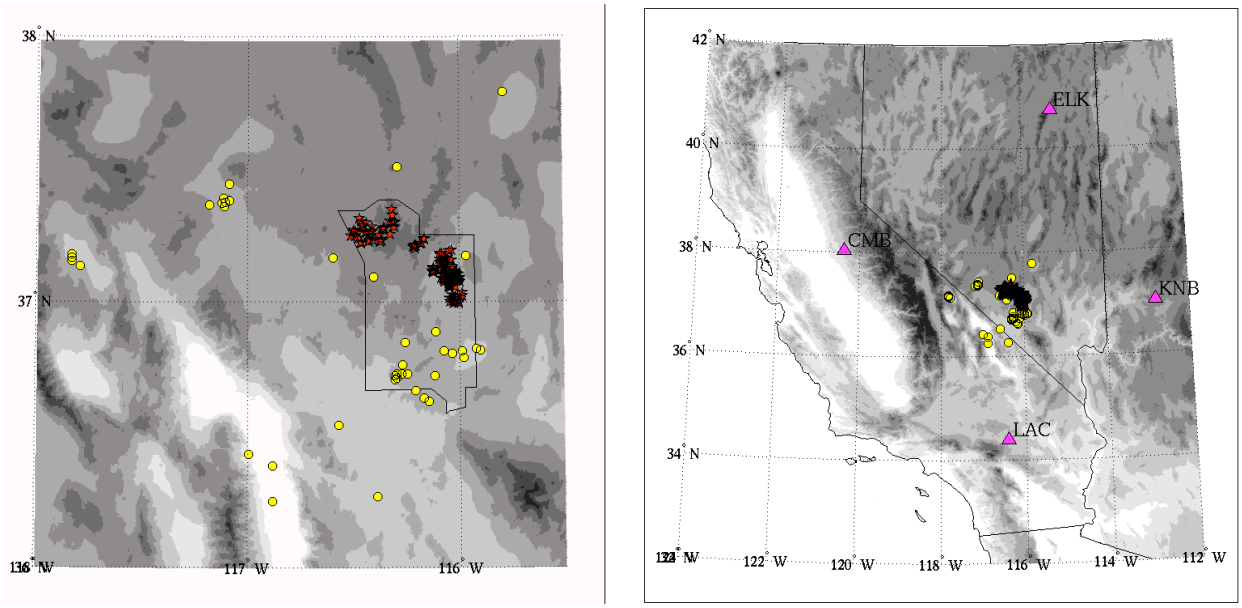

Fig. 1. Maps of NTS events observed at regional distances by stations KNB, ELK, LAC and CMB. Explosions are red and earthquakes are yellow.

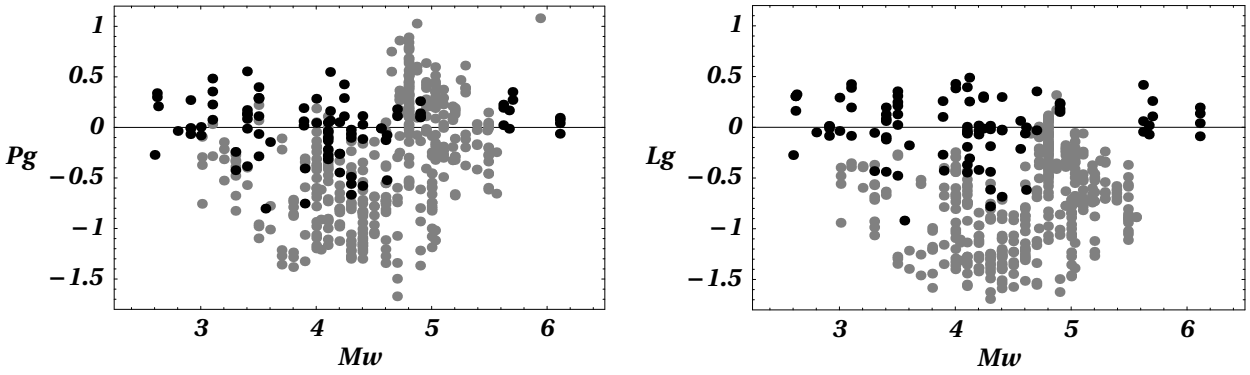

Fig. 2. Scatter plots of MDAC corrected amplitudes L_g and P_g versus moment magnitude M_w for earthquakes (dark) and explosions (light). MDAC corrects earthquakes to zero mean.

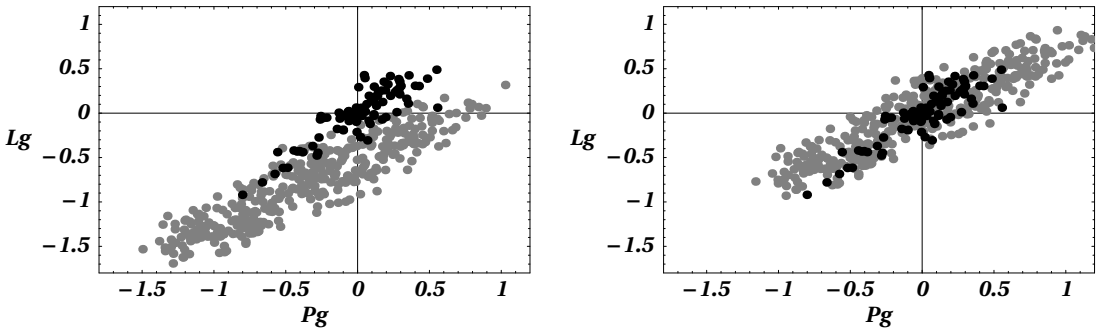

(a) L_g versus P_g.

(b) L_g versus P_g with the explosion and earthquake data mean centered.

Fig. 3. Scatter plots of the MDAC corrected amplitudes L_g versus P_g for earthquakes (dark) and explosions (light). Figure 3(a) exhibits discrimination because the earthquake and explosion populations are disjoint. With the explosions mean centered, Figure 3(b) shows the data that are used to calibrate the common standard error parameters (τ and σ for P_g and L_g, and ρ) for both populations.

Table 1. Estimates of Model Error (τ^2) and Station Error (σ^2) for MDAC corrected P_g and L_g amplitudes. From Figure 6, the estimated correlation between P_g and L_g is $\rho = 0.95$.

Phase	Model Error	Station Error
P_g	0.23	0.04
L_g	0.16	0.02

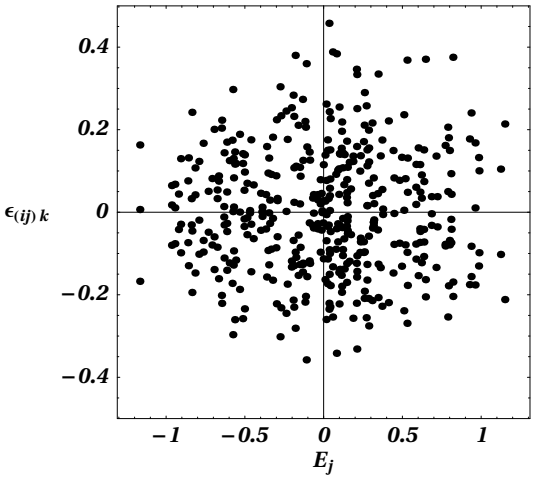

(a) Fitted model terms E_j and $\epsilon_{(ij)k}$ for P_g.

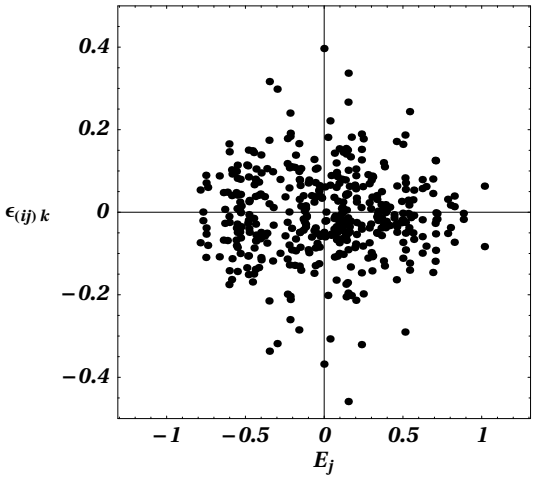

(b) Fitted model terms E_j and $\epsilon_{(ij)k}$ for L_g.

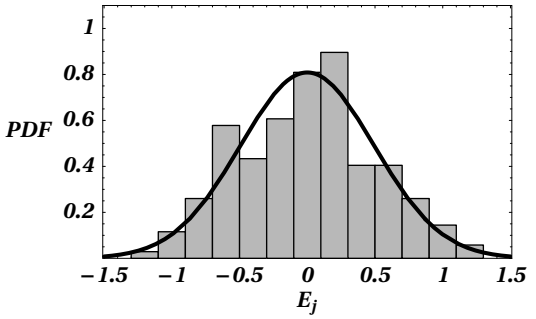

(c) Histogram and fitted PDF of E_j for P_g. A goodness-of-fit test returned $\chi^2 = 10.80$ with 13 degrees of freedom and p-value $= 0.63$.

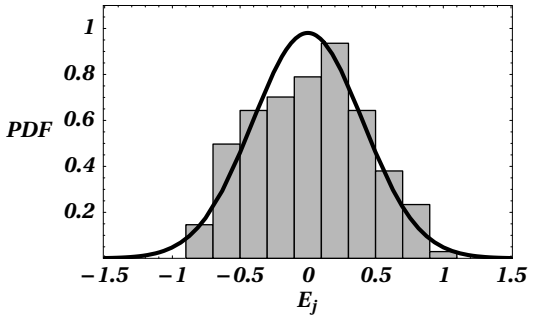

(d) Histogram and fitted PDF of E_j for L_g. A goodness-of-fit test returned $\chi^2 = 10.45$ with 13 degrees of freedom and p-value $= 0.66$.

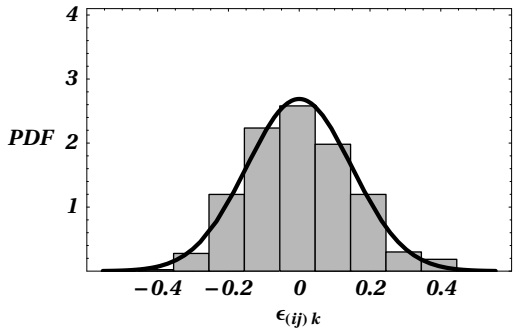

(e) Histogram and fitted PDF of $\epsilon_{(ij)k}$ for P_g. A goodness-of-fit test returned $\chi^2 = 10.88$ with 9 degrees of freedom and p-value $= 0.28$.

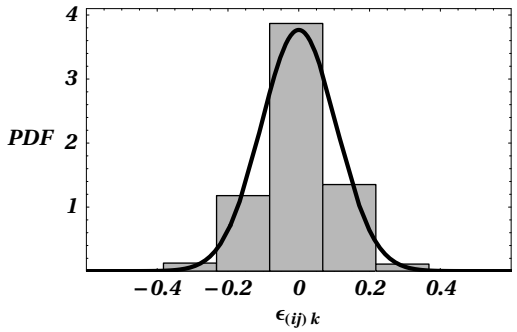

(f) Histogram and fitted PDF of $\epsilon_{(ij)k}$ for L_g. A goodness-of-fit test returned $\chi^2 = 28.73$ with 7 degrees of freedom and p-value ≈ 0.

Fig. 4. Validation analysis for the distributional properties of E_j and $\epsilon_{(ij)k}$ for the MDAC multi-station discriminant. The MDAC model assumptions specified in Equation (6) are normality and independence of E_j and $\epsilon_{(ij)k}$. χ^2 goodness-of-fit tests were performed with the bin size chosen to give a best fit to a normal distribution. For each test, the degrees of freedom include subtraction of an additional degree of freedom to account for model parameter estimation (τ, σ). All tests constrain the PDF mean to zero.

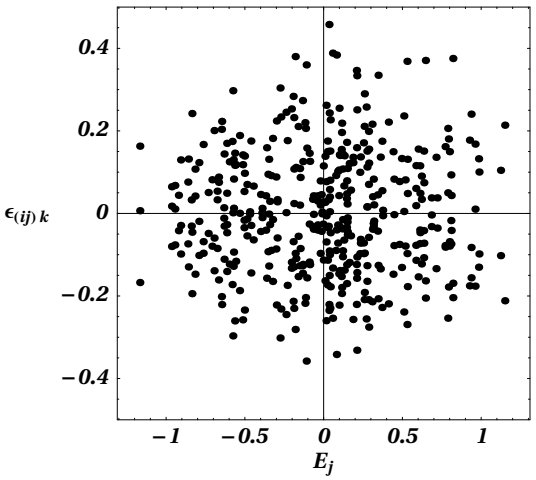

(a) Fitted model terms E_j and $\epsilon_{(ij)k}$ for P_g.

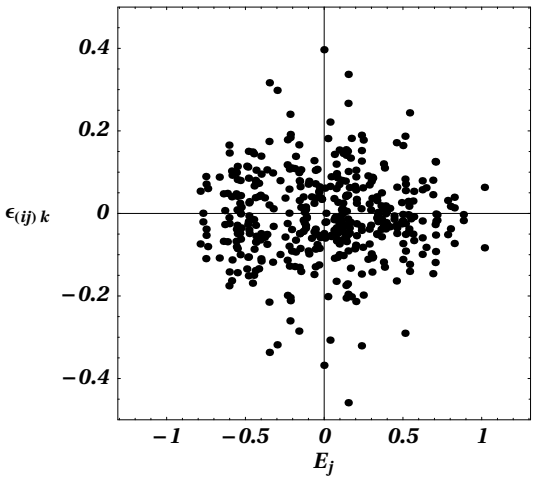

(b) Fitted model terms E_j and $\epsilon_{(ij)k}$ for L_g.

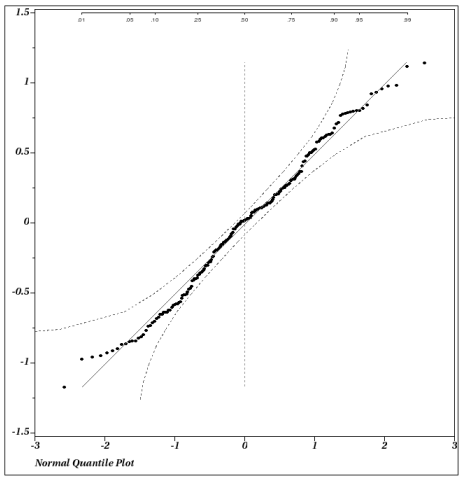

(c) Q-Q plot of E_j for P_g.

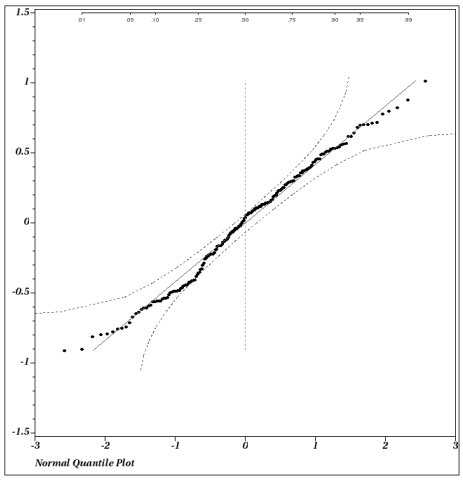

(d) Q-Q plot of E_j for L_g.

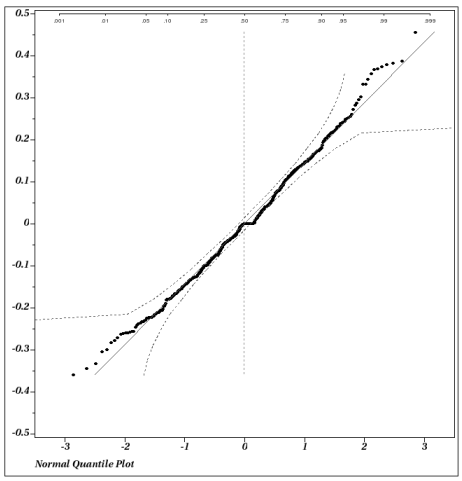

(e) Q-Q plot of $\epsilon_{(ij)k}$ for P_g.

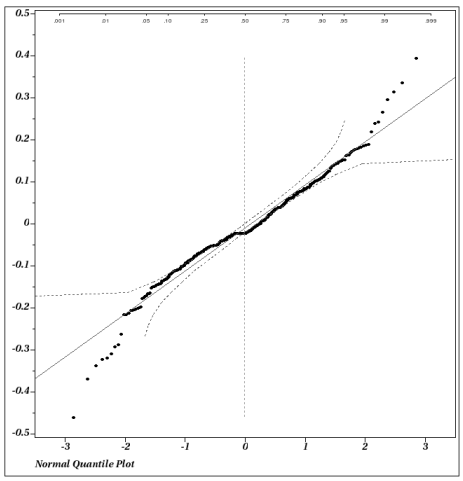

(f) Q-Q plot of $\epsilon_{(ij)k}$ for L_g.

Fig. 5. Validation analysis for the distributional properties of E_j and $\epsilon_{(ij)k}$ for the MDAC multi-station discriminant. The MDAC model assumptions specified in Equation (6) are normality and independence of E_j and $\epsilon_{(ij)k}$. The normal quantile-quantile (Q-Q) plots for E_j and $\epsilon_{(ij)k}$ include 95% confidence bounds assuming a normal distribution.

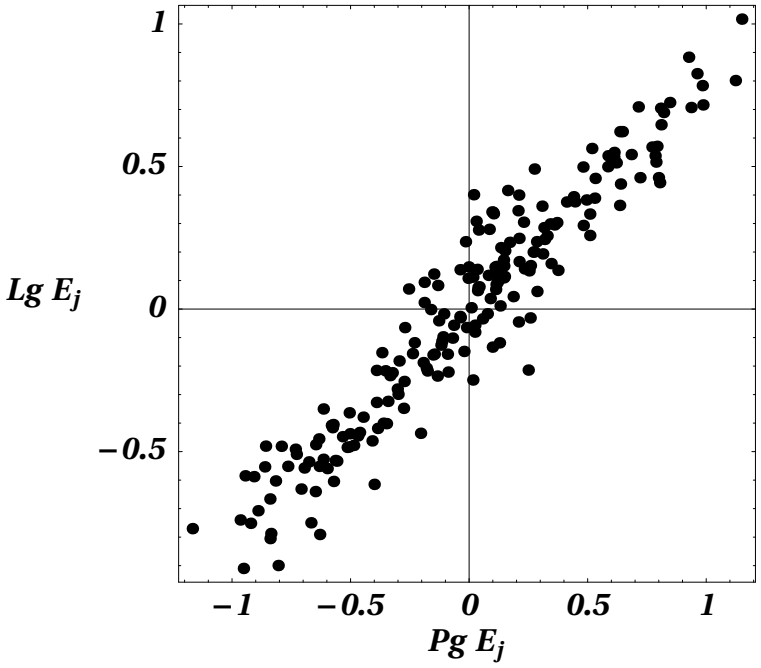

Fig. 6. Bivariate plot of fitted E_j values for P_g and L_g. The calculated correlation $\rho = 0.95$. The MDAC correction removes magnitude from amplitudes and so ρ is the correlation between amplitude *error* terms E_j. Thus an observed model inadequacy $P_g\ E_j$ is linearly related to observed $L_g\ E_j$ with ρ indicating the scatter around the line of the relationship.

Table 2. Source type bias (average) for MDAC corrected P_g and L_g amplitudes.

Bias	EX $(i = 1)$	EQ $(i = 0)$
μ_{P_g}	-0.34	0
μ_{L_g}	-0.76	0

Table 3. Identification performance of the MDAC multi-station discriminant in Equation (13) with the model-based decision line $\ell_{Model} = -0.89$. Rows are true source-type and columns are identified source.

	$\hat{EX}$	$\hat{EQ}$
EX	137	22
EQ	1	40

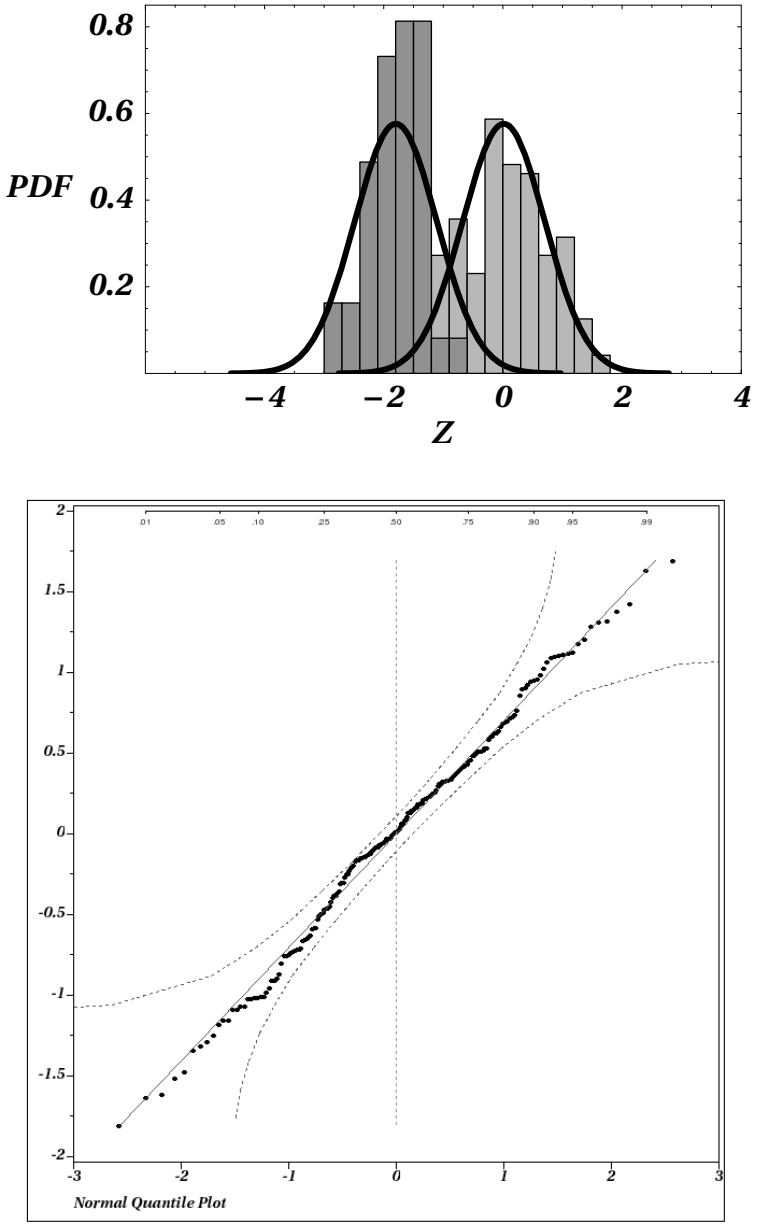

Fig. 7. Fitted models of the multi-station MDAC discriminant $Z_{\bar{P}_g - \bar{L}_g}$ for earthquakes (dark) and explosions (light). The explosion population mean is ≈ 0 and the earthquake population mean is -1.80. The pooled standard deviation for the populations is 0.69. The Q-Q plot is of the pooled earthquake and explosion data (centered to their respective source type means), and it confirms that the earthquake and explosion data are reasonably modeled as normal with equal variance.

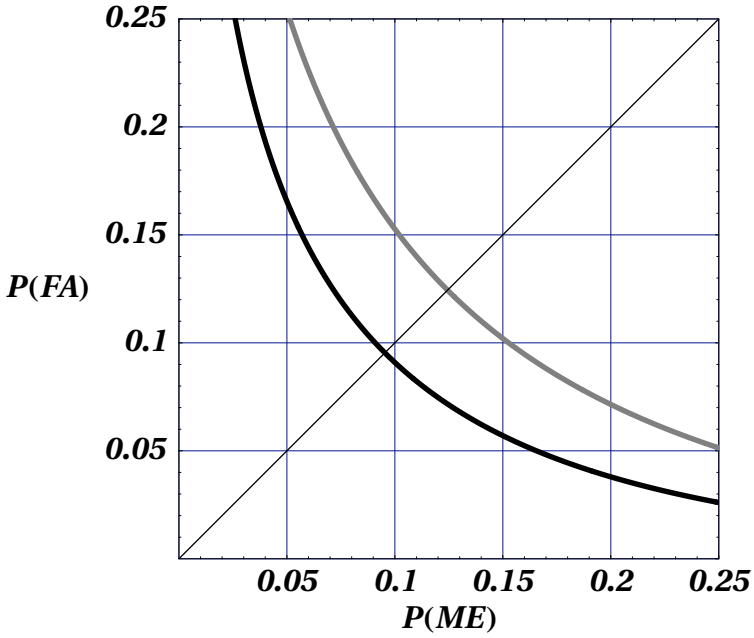

Fig. 8. Receiver operation curves (ROC) for multi-station MDAC (dark) and multi-station regression correction (light) discrimination. The equi-probable error, identified by the 45 degree line is $\approx 10\%$ for MDAC discrimination and $\approx 12.5\%$ for regression discrimination. FA denotes false-alarm and ME denotes missed explosion.

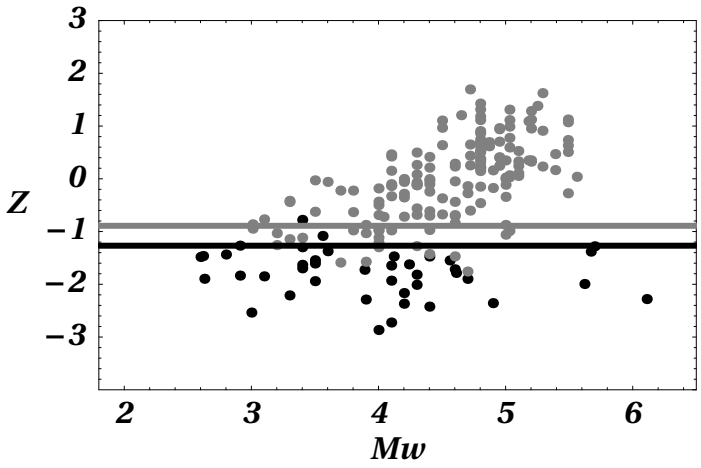

Fig. 9. Scatter plot of observed MDAC multi-station discriminants versus M_w. Earthquakes are dark and explosions are light. The decision thresholds are $\ell_{Model} = -0.89$ (light) and $\ell_{Empirical} = -1.27$ (dark). Performance counts are reported in Tables 3 and 4.

Table 4. Identification performance of the MDAC multi-station discriminant in Equation (13) with the empirical-based decision line $\ell_{Empirical} = -1.27$. Rows are true source-type and columns are identified source.

	$\hat{EX}$	$\hat{EQ}$
EX	152	7
EQ	2	39

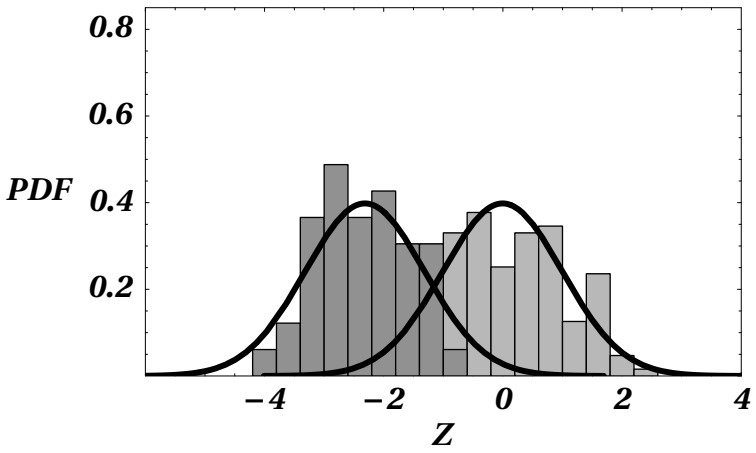

Fig. 10. Fitted models of the multi-station regression correction discriminant $Z_{\bar{X}}$ for earthquakes (dark) and explosions (light). The explosion population mean is ≈ 0 and the earthquake population mean is -2.32. The pooled standard deviation for the populations is 1.00.

Table 5. Estimates of Model Error (τ^2) and Station Error (σ^2) for the regression corrected station discriminants $X = P_g - L_g$.

Station Discriminant	Model Error	Station Error
$X = P_g - L_g$	0.009	0.034

Table 6. Source type bias (average) for the regression corrected station discriminant $X = P_g - L_g$.

Bias	EX $(i = 1)$	EQ $(i = 0)$
μ_X	0.368	0

Table 7. Identification performance of the regression correction multi-station discriminant in Equation (16) with the model-based decision line $\ell_{Model} = -1.16$. Rows are true source-type and columns are identified source.

	$\hat{EX}$	$\hat{EQ}$
EX	135	24
EQ	3	38

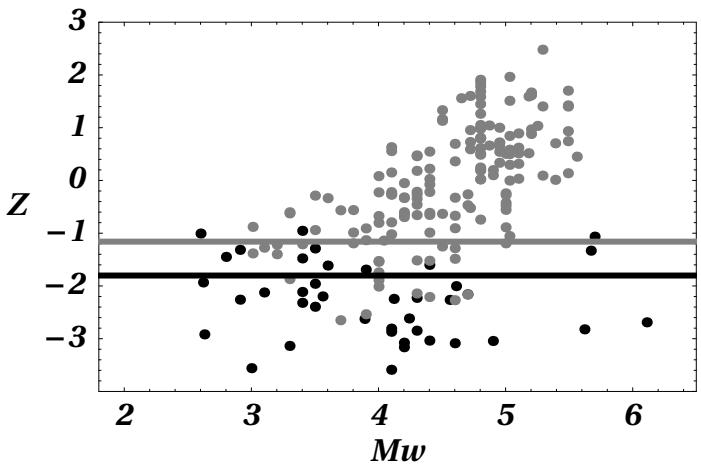

Fig. 11. Scatter plot of observed regression corrected multi-station discriminants versus M_w. Earthquakes are dark and explosions are light. The decision thresholds are $\ell_{Model} = -1.16$ (light) and $\ell_{Empirical} = -1.80$ (dark). Performance counts are reported in Tables 7 and 8.

Table 8. Identification performance of the regression corrected multi-station discriminant in Equation (16) with the empirical-based decision line $\ell_{Empirical} = -1.80$. Rows are true source-type and columns are identified source.

	$\hat{EX}$	$\hat{EQ}$
$\boldsymbol{EX}$	150	9
$\boldsymbol{EQ}$	11	30

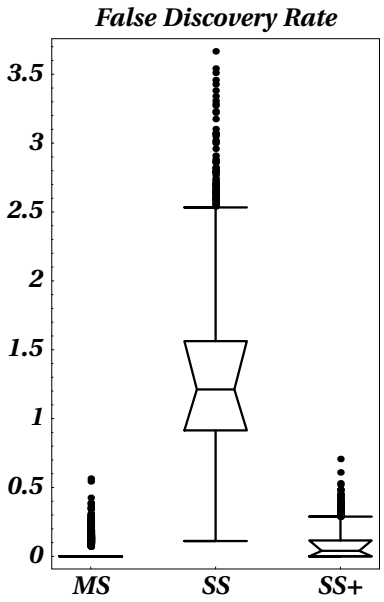

Fig. 12. Boxplots of 5000 cross-validated values of the FDR for the multi-station (MS) discriminant, and the single-station (SS) and single-station plus (SS+) approaches to regional discrimination.

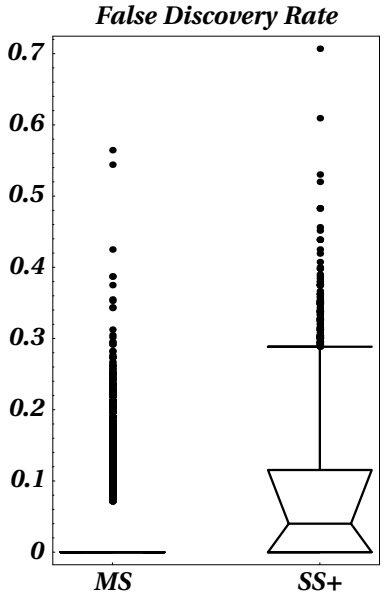

Fig. 13. Boxplots of 5000 cross-validated values of the FDR for the multi-station (MS) discriminant and the single-station plus (SS+) approaches to regional discrimination.

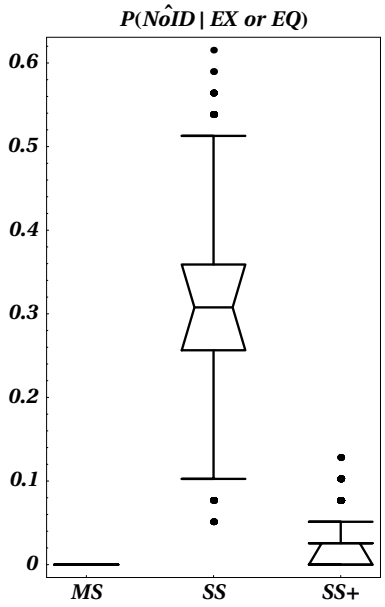

Fig. 14. Operational Burden for the multi-station (MS) discriminant, and the single-station (SS) and single-station plus (SS+) approaches to regional discrimination. Boxplots are from 5000 cross-validated values of the $P(\hat{NoID} \mid EX) + P(\hat{NoID} \mid EQ)$ component of Operational Burden.

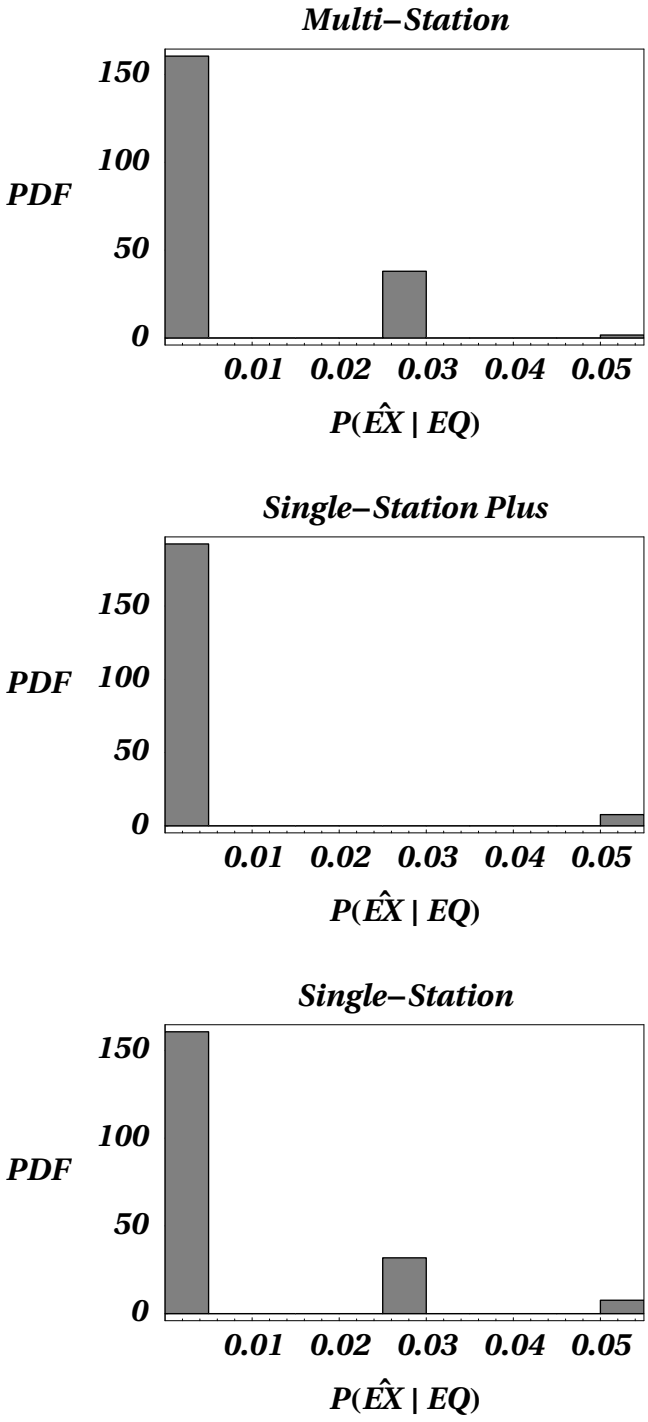

Fig. 15. Operational Burden for the multi-station discriminant, and the single-station and single-station plus approaches to regional discrimination. Histograms are from 5000 cross-validated values of the $P(\hat{EX} \mid EQ)$ component of Operational Burden.

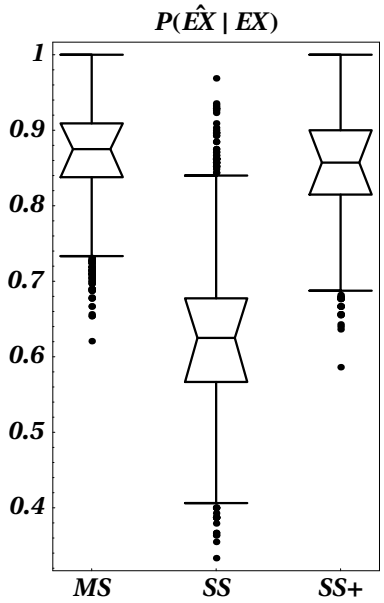

Fig. 16. Boxplots of 5000 cross-validated values of $P(\hat{EX} \mid EX)$ for the multi-station (MS) discriminant, and the single-station (SS) and single-station plus (SS+) approaches to regional discrimination.